Ambient Backscatter Communications in Mobile Networks: Crowd-Detectable Zero-Energy-Devices

Dinh-Thuy Phan-Huy, Dominique Barthel, Philippe Ratajczak, Romain Fara, Marco Di Renzo, Julien de Rosny

Ambient Backscatter Communications in Mobile Networks: Crowd-Detectable Zero-Energy-Devices

Dinh-Thuy Phan-Huy[1], Dominique Barthel[1], Philippe Ratajczak[1], Romain Fara[1, 2], Marco di Renzo[2], Julien de Rosny[3]
[1]*Orange Innovation*, Châtillon, Meylan & Sophia-Antipolis, France
[2]*Université Paris-Saclay, CNRS, CentraleSupélec, Laboratoire des Signaux et Systèmes*, Gif-Sur-Yvette, France
ESPCI Paris, PSL University, CNRS, Institut Langevin,75005 Paris, France
{dinhthuy.phanhuy, dominique.barthel, philippe.ratajczak}@orange.com, fararomain@gmail.com, marco.di-renzo@universite-paris-saclay.fr, julien.derosny@espci.fr

***Abstract*—In this paper, we introduce the new concept of Crowd-Detectable Zero-Energy-Devices. Such devices harvest solar or ambient light energy to power themselves, backscatter ambient waves to communicate, and are detected simultaneously by a smartphone connected to the network, and by the network itself, as long as the device is close to the considered smartphone. Such a device is a promising sustainable solution for the future of the Internet of Things. We describe an example of use case: asset tracking with zero added energy, zero new signals and zero new infrastructure in the network, thanks to the anonymous and transparent participation of smartphones connected to the wireless network. We then present our first prototypes of such devices that backscatter TV, 4G and 5G signals, and show our first experiments in challenging conditions and environments.**

Keywords—Ambient backscatter communications; 4G; 5G; 6G; RF tag; Internet of things.

I. INTRODUCTION

Each generation of mobile networks, from the 2nd generation (2G) to the 5th generation (5G) has been improved in terms of spectral and energy efficiency. Nevertheless, due to the fast traffic demand growth, the network energy consumption keeps growing [1]. Hence, there is a strong need for finding sustainable solutions for wireless communications. Recently, ambient backscatter communications have been proposed [2]. In such communication systems, a tag sends a message to a reader without generating any radiofrequency (RF) wave. It backscatters ambient waves generated by an external source such as a television (TV) tower. In [3], such a system has been identified as a promising solution for Internet of Things (IoT) applications. In [4], real-time ambient backscatter communications have been demonstrated with a first tag prototype backscattering TV or 4th generation (4G) network waves and harvesting solar energy to power itself. However, the presented prototype was bulky and therefore very far from a product in terms of form factor. In [5], the experimental characterization of the performance of such link with the most basic detector (an energy detector) has been performed, showing that performance fades in some localized areas. In [6-10], solutions to improve the performance have been proposed, by using massive multiple-input multiple-output (M-MIMO) antennas at the reader side [6] or at the source side [7], by using compact reconfigurable backscatters in polarization [8,9], or by assisting the communication with a reconfigurable intelligent surface in the context of a future 6th generation (6G) network [10].

However, up to now, no use case strongly attractive to mobile operators has emerged. In this paper, for the first time, we introduce, in Section II, the concept of crowd-detectable zero-energy-device (CD ZED), based on ambient backscatters in mobile networks. We present the new and very promising use case of "asset tracking out-of-thin-air" in Section III. We also present our first prototypes in Section IV. Finally, in Section V, we describe some first experimentations and demonstrations presented at the 2021 Orange Labs Research Exhibition [11] and the 2021 Mobile World Congress [12].

II. CD ZED CONCEPT

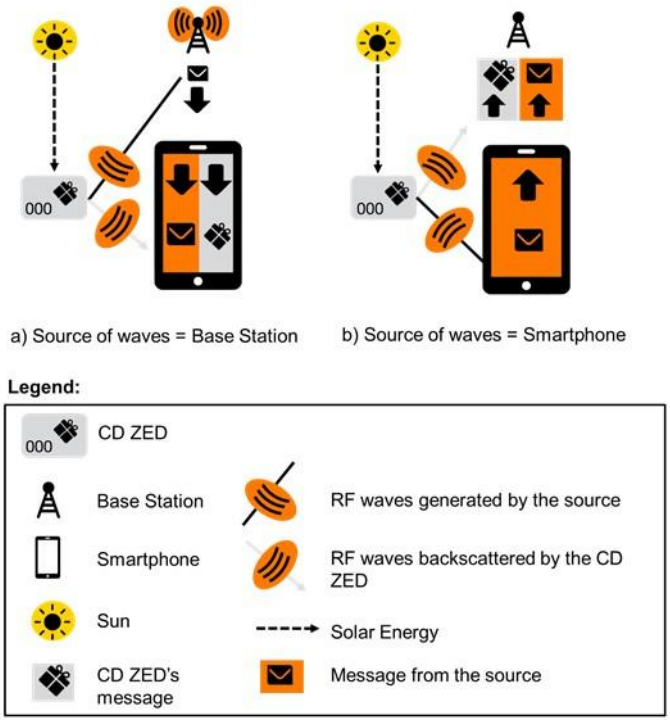

Fig. 1. CD ZED concept

A CD ZED harvests solar or ambient light energy to power itself, backscatters ambient waves to communicate, and is detected simultaneously by a smartphone connected to the network, and by the network itself, as long as the device is close to the considered smartphone. As illustrated in Fig. 1, each time a CD ZED gets close to a smartphone connected to the network, it backscatters the waves that are generated by the network and that are intended for the smartphone. Simultaneously, it backscatters the waves that are generated by the smartphone and that are intended for the network. The smartphone can simultaneously demodulate the data coming from the network and act as a RF tag reader, by detecting the tag message through an analysis of the propagation channel variations. Similarly, the network can simultaneously demodulate the signal coming from the network, plus act as a RF tag reader, by detecting the tag's message in the channel variations. Hence, the tag's detection can be associated with the smartphone location. In other terms, when a tag gets close to a smartphone, it is automatically located and time-stamped by the smartphone and the network.

By organizing anonymous participation of all its smartphone customers, an operator can therefore track the locations of any tags that "bump" into one member of its "crowd" of smartphones. To protect its smartphone customers' personal data, it is important that the mobile operator collects the participation agreement from each customer (through an electronic form for instance). This agreement must include guarantees from the operator that the customer's participation will remain completely anonymous. More precisely, once a tag is detected, located, and time-stamped, neither personal data linked to the smartphone nor the customer identity must be stored.

Such a device is a promising sustainable solution for the future of the IoT. Indeed, it enables a mobile network operator to develop IoT use cases without spending more energy, without emitting new waves, and without deploying additional infrastructure in the network.

III. ASSET-TRACKING OUT-OF-THIN-AIR

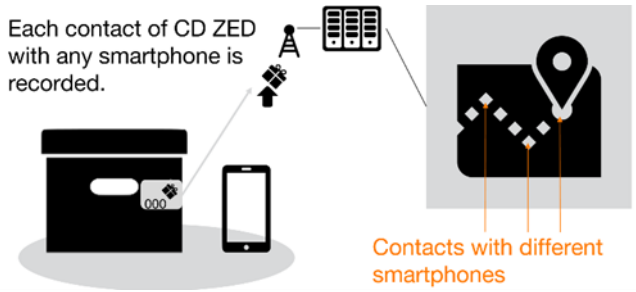

Fig. 2. Asset tracking with zero added energy, zero new signals and zero new equipment in the network

In this section, we describe a promising use case: "Asset-Tracking Out-of-Thin-Air", i.e., asset tracking with zero added energy, zero new signals, and zero new infrastructure in the network. As illustrated in Fig. 2, a shipping company puts a CD ZED on a package. Each time the package gets close to a smartphone, it is automatically located and time-stamped by the network. Thanks to the anonymous and transparent participation of smartphones connected to the wireless network (described in Section III), the trajectory of the package can be tracked even in outdoor environments or other situations where no Radio Frequency Identification (RFID) portals or readers are deployed.

To illustrate the anonymous participation of smartphone customers for tracking-out-of-thin air, we propose to describe hereafter a protocol example that could be used with current 4G mobile networks. Indeed, 4G networks have been standardized by the 3rd generation partnership project (3GPP)[13] and are mature networks with national coverages in many countries. A similar protocol can be derived for 5G.

First of all, the customer would install a CD-ZED app on its smartphone. The smartphone is called user equipment (UE) in the standard. This app would connect the UE to a server, located in the Evolved Packet Core (EPC) of the mobile network operator. Let us call this server the CD-ZED server. Then, the CD-ZED server would be informed of the detection of a tag according to two different operating modes: the downlink and the uplink operating mode, detailed hereafter.

In the downlink operating mode (illustrated in Fig. 1-a), as already defined in current 4G standards, the smartphone would monitor the 4G base station (BS) following common signals (sent within a 1 ms sub-frame) [13]: downlink pilots called Reference Signals (RS) sent in every ms, the Primary Synchronization (PSCH) and the Secondary Synchronization Channels (SSCH) sent every 5 ms, the Broadcast Channel (BCH) sent every 10 ms, the Physical Downlink Control Channel (PDCCH) sent every ms. In addition, the UE would also demodulate the Physical Downlink Shared Channel (PDSCH) (upon reception of a control message in the PDCCH indicating incoming data). In addition to these already standardized tasks, the UE would perform the following tasks. First, it would process the received data or control symbols to extract the tag's message: the tag identity (ID). For instance, the UE could simply compute the symbols' powers and apply an energy detector as detailed in Section V. Then, the UE would forward the received tag ID to the CD-ZED server (through the radio access network and then the EPC) along with the identity of the smartphone, i.e., the User Equipment (UE) ID.

In the uplink operating mode (illustrated in Fig. 1-b), as already defined in current 4G standards, the BS would monitor the UE standardized uplink control signals (sent within a 1 ms sub-frame) [13]: the Sounding Reference Signals (SRS) sent every 5 ms or more, the Physical Uplink Shared Channel (PUSCH) sent to transport uplink data, and the Physical Uplink Control Channel (PUCCH), sent to report information regarding the UE buffer, to report a radio Channel Quality Indicator (CQI), to request uplink data transmission, or other control signaling messages. In addition to these already standardized tasks, the BS would perform the following tasks. First, it would process the

received data or control symbols to extract the tag ID. Then, the BS would forward the received tag ID to the CD-ZED server (through the EPC) along with the UE ID.

In parallel, the CD-ZED app running on the UE would call a geolocalisation service based on the 3GPP standard and/or an app based on global navigation satellite systems (GNSS) such as Global Positioning System (GPS) (an over-the-top application out of 3GPP standard). Hence, the CD-ZED server would receive UE positions from the standardized 3GPP Localization Service (LCS) function [14] and/or the GNSS-based app. We remind that the LCS function monitors the position of the UE by collecting inputs from the standardized positioning functionalities of 2G, 3G, and 4G radio interfaces. Upon reception of the UE ID and the tag ID, the CD-ZED would time stamp the received tag ID and associate this tag ID to the current position of the UE corresponding to the received UE ID. Then, the CD-ZED server would update the tag tracked trajectory by adding this new time-stamped position to other previously recorded ones.

Finally, the CD-ZED server would erase the UE ID as this information would no longer be useful. Hence, the participation of the customer in the tracking of the tag would remain anonymous.

Note that, in this example, no additional hardware is needed on the UE side nor the BS. However, firmware modifications, in the baseband processing, are necessary to extract the tag's message from the already received symbols. Most importantly, as illustrated by the previously described protocol example, significant evolution of the 3GPP standard is required.

IV. Zero-Energy-Device Prototypes

In this section, we present our first prototypes of CD ZEDs: compact solar tags with a fixed message.

A. Overview

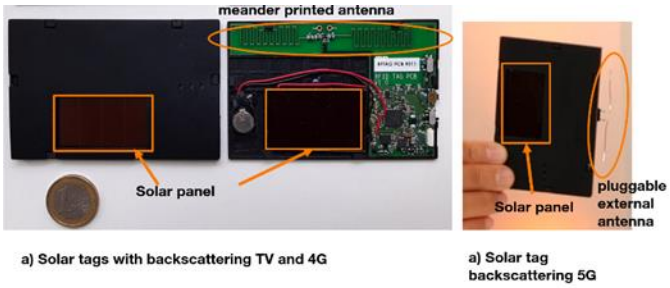

Fig. 3. Prototypes of CD ZEDs: business card size solar tags recycling TV/4G (between 480 and 800 MHz) and 5G signals (at around 3.5 GHz)

Our tag is the size of a business card and is mainly composed of a dipole antenna connected to an RF switch, itself being controlled by a MSP430. A BQ25570 Power Management Integrated Circuit (PMIC) is used to harvest microwatt energy from an indoor solar panel AM-1454CA, store it into a 3 V coin cell battery and deliver a regulated voltage to the tag transmitter. Hence, a tag self-powers with solar or ambient indoor light. A tag repeatedly sends a black and white pixel image of 8 rows and 11 columns (88 pixels in total), each black or white pixel being coded by a bit. A synchronization sequence of 8 bits is prepended to the 88 bit-sequence corresponding to the image. The whole 96-bit sequence is sent using FM0 modulation as in [2], hence with 96×2=192 FM0 bits. The RF switch connects together the two branches of the dipole when the FM0 bit is equal to zero and disconnects them otherwise. Displaying this 88-pixels image in real-time enables us to visualize the raw bit error rate (BER) (i.e. the BER without channel coding) in real time during experiments on the fields. When one pixel is wrong, the BER is around 10%, when all pixels are correct, the BER is below 10%. In particular, by watching at the quality of the received image (while increasing the distance between the tag and the reader) we can find the maximum tag-reader range very rapidly.

Depending on the impedance that loads the dipole antenna, the tag backscatters a different level of ambient field. To guarantee a good contrast between the two states, we have chosen the Infineon BGS12WN6 wideband SPDT Diversity Switch that provides high isolation and low insertion loss at frequencies below 6 GHz, even under a supply voltage as low as 2.0 V. Finally, the tag's rate is computed as follows. The tag switches every Ts seconds, sends Fs=1/Ts FM0 symbols per second and Fb=1/(2 Ts) bits (or pixels) per second. The setting of Ts depends on the ambient source. For instance, in 5G, Ts must be set to a larger value that the Time Division Duplex frame duration T_5G of 1 ms, to avoid any confusion between the tag's symbol period and the frame period. Ts setting for each type of ambient source is detailed in Section V.

As in [2], though it is not optimal, the FM0 modulation has been chosen to perform ambient backscatter communications real-time experiments on the field. First, it is very low-complexity and low-energy. Secondly, it is detectable by a Software Defined Radio (SDR) prototype of reader, which is running a low-complexity energy-detector in real-time.

Future studies will consider more sophisticated modulations such as Binary phase-shift keying (BPSK) for backscatters as in [15] (or Minimum Shift Keying), as it is the most energy-efficient modulation, or direct-sequence spread spectrum (DSSS) for backscatters as in [16]. Especially, in studies not necessarily requiring real-time detection, more advanced receivers (similar to those running on commercial smartphones or BSs) using multiple antennas as in [17] will be studied.

B. Antenna

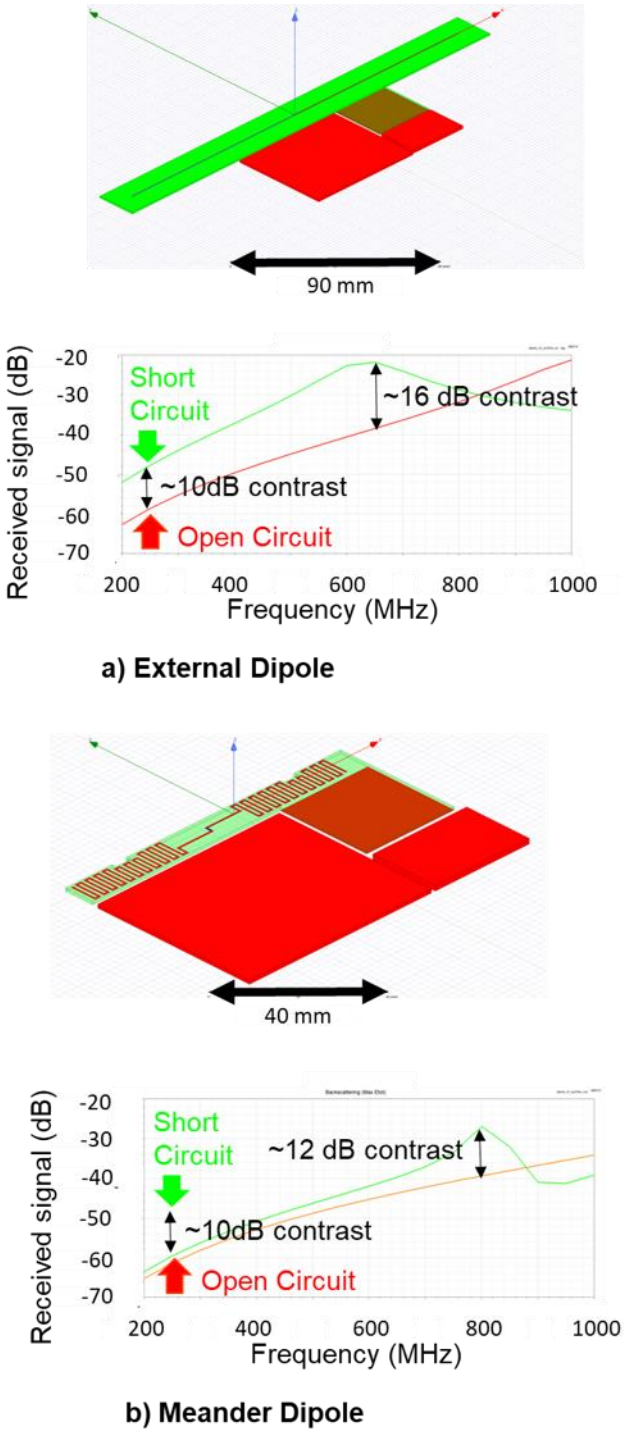

Fig. 4. Full-wave simulation using HFSS of (a) external pluggable dipole antenna based tag and (b) meander antenna based tag.

Regarding the dipole antennas, two options are available. Either a printed meander antenna as illustrated in Fig. 3-a) or an external pluggable dipole antenna is used as illustrated in Fig. 3-b). Fig. 4-a) and Fig. 4-b) illustrate the external dipole antenna-based tag and the meander antenna-based tag solutions, respectively. Fig. 4 also includes plots of the corresponding reflected signals at the reader side, when the tag is in short-circuit or open circuit state, respectively, using a High Frequency Simulation Software (HFSS) tool. In these simulations, the source and the reader are dipole antennas located above the tag, in the boresight of the antenna of the tag, with the same polarization as the tag, to maximize the tag's detection. As illustrated in Fig. 4), the advantage of the dipole is that the contrast between the two states is higher and the bandwidth in which the contrast is significant is larger. The drawback of this solution is the size of the tag (it reaches around 20 cm at 700 MHz). The meander-based antenna tag is advantageously more compact. However, the contrast of the meander antenna is weaker and the bandwidth in which the contrast is significant is much narrower. To be able to use the tag over a large frequency band, the meander antenna must be designed for the higher working frequency, and then by adding an inductance on each arm of the meander (as illustrated in Fig. 5-a), a lower working frequency (900 MHz to 500 MHz) can be tuned thanks to the inductances (0 nH to 50 nH) that artificially lengthen the meander (as illustrated in Fig. 5-b) to g). To widen the frequency band, a co-design of the tag circuit and antenna parts is needed to keep space on the whole tag surface for the integrated antenna, in order to maintain the antenna size as large as possible.

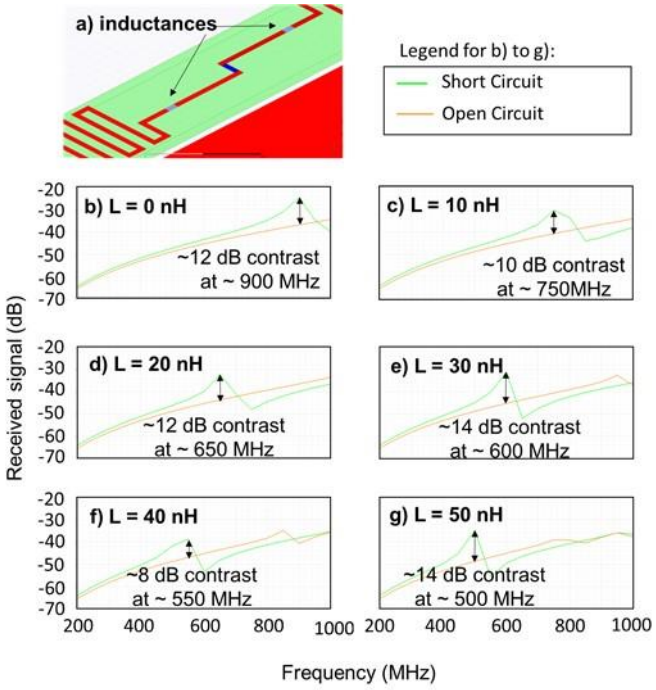

Fig. 5. Full-wave simulation using HFSS of a meander antenna based tag with impedances L located at positions illustrated in (a), for L equal to b) 0 nH, c) 10 nH, d) 20 nH, e) 30 nH, f) 40 nH and g) 50 nH.

C. Energy balance

In this subsection, we estimate the energy balance of the tag, following this two-step approach: 1) evaluating the power that the tag can harvest thanks to the solar panel, when the tag is "off" (i.e. the communication subsystem constituted of the MSP430, the visual feedback LEDs, and the RF switch, is not activated);

2) evaluating the power that is spent by the tag when the tag is "on" (i.e. the communication subsystem is activated), and the energy harvesting is not activated. Comparing these two power values, we can compute the device lifetime under various conditions.

Our prototype was designed to allow disabling various subsystems, so that this two-step experimental validation can be performed. More precisely, Fig. 6 shows a block diagram of the energy management of the tag. The battery provides energy to the MSP430, LEDs and RF-switch subsystem via the voltage regulator. Switch SW2 enables or disables the output voltage regulator of the PMIC. When SW2 is set to "off", the tag voltage regulator is turned off, its output drops to 0 V, the MSP430, LEDs and the RF switch no longer draw any current from the battery. The battery receives energy from the solar panel or from an External_Vin input connector, via the battery charger. Switch SW4 selects the input. If External_Vin is left unconnected and SW4 is set to External_Vin, no energy will be provided to the battery charger and the battery will not charge at all, even though the charger is still powered internally. Note that the battery charger and the voltage regulator of Fig. 6 are actually part of the same PMIC. To measure the energy consumption of the tag transmitter alone, without the PMIC being considered, the MSP430, LEDs and RF switch subsystem may be powered from the 2V0 input connector.

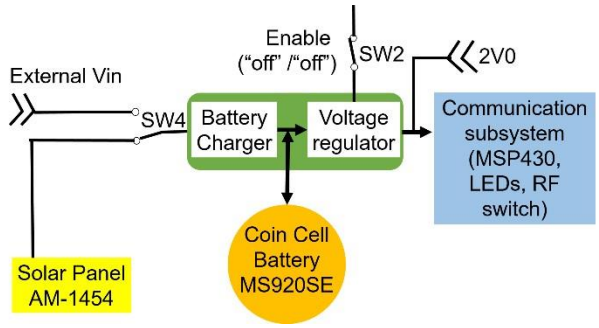

Fig. 6. Tag energy management

As announced above, we first study the ability of the tag to harvest light energy thanks to the solar panel, under various lighting conditions, when the tag is "Off". The power/energy measurements are conducted at the battery positive terminal using an OTII ARC power source/monitor by Qoitech and an HP 34401A Digital Multimeter. Our energy test setup is illustrated in Fig. 7. A shunt resistor is inserted in series with the positive (red) wire of the battery. It provides a [-3.7 mA, +3.7 mA] measurement range, and a resolution of 0.1 µA. All measurements were performed at room temperature, with the SW4 set to "solar panel". The measurements are collected in Table I.

TABLE I. BATTERY CHARGE MEASUREMENTS

	200 lux	"medium"	"bright"	1000 lux
Solar panel output (specification)	45 µW			250 µW
Battery charging power (measured)		45 µW	150 µW	
Time from empty to full charge (extrapolated)		1 month	9 days	

For this rapid validation, we did not have a luxmeter handy, therefore the values reported are only ballpark estimates. Under "medium" indoor lighting conditions, the measured current is 15 µA, corresponding to about 45 µW since the battery voltage was measured to be 3.0 V at that time. This value corresponds to the nominal specification of the AM-1454 solar panel at a light level of 200 lux. Under "bright" indoor lighting, we measured 150 µW. As a reference point, the expected power for the AM-1454 at 1000 lux is about 250 µW. It follows that an ideal 11 mA·h 3.0 V battery (i.e., 120 Joules), initially empty, would need 9 days to fully charge out of the solar panel under bright light (i.e., with 150 µW), and a month under nominal light (i.e., with 45µW). In practice, we can say that fully charging a deeply discharged MS920SE battery out of the solar panel would take from days to weeks depending on the light intensity.

The PMIC adapts to the lighting conditions to extract the maximum power available, thanks to its internal Maximum Power Point Tracking (MPPT) mechanism: every 16 seconds, the battery charger disconnects the solar panel for 250 ms to sense its open-circuit voltage, then operates the charger for the next 16 seconds in a closed loop such that the solar panel operating voltage is a fixed ratio of the sampled open-circuit voltage. This ratio is user-defined to match the solar panel characteristics, a typical value being 0.8. This MPTT operation is witnessed on Fig. 8 where, after a period of low lighting, bright light is applied to the solar panel : a smartphone torch is placed in front of the solar panel, at an approx. 10 cm distance. The purple curve on Fig. 8 shows that the current immediately jumps to about -30 µA (battery charging) as the bright light is applied. Then, at the next sensing phase, the MPTT mechanism adjusts the charger parameters for the new lighting conditions, and the current further jumps to -50 µA.

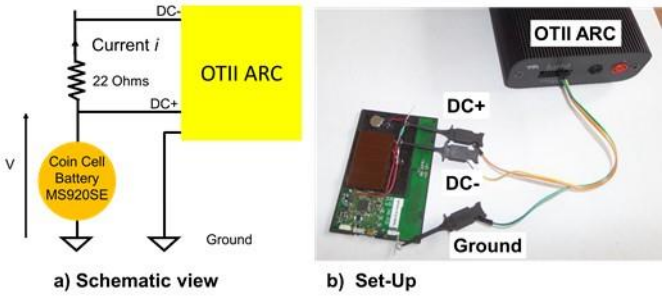

Fig. 7. Set-up for the measurement of the current *i*

We now study the tag energy consumption when energy harvesting is not activated. Our tag prototype can operate in one of several modes (selected using a push button), including: the "Deep Sleep" mode, during which the RF tag is alert to button presses but does not transmit any data; the "Permanent Sending" mode, during which the RF Tag continuously sends the same sequence of data, back-to-back. In this study, the SW4 switch is

set to External_Vin and nothing is connected to External_Vin. Therefore, there will be no current coming from the battery charger into the battery. This allows us to properly measure the discharge currents, including that of the PMIC itself. Again, all measurements were done at room temperature.

TABLE II. BATTERY DISCHARGE MEASUREMENTS

	Deep Sleep	Permanent
Battery discharging power (measured)	2.3 µW	250 µW
Time from full to empty battery (extrapol.)	1.7 years	5.6 days

The RF Tag prototype consumes about 2.3 µW and 250 µW in Deep Sleep and Permanent Sending modes, respectively, see Table II.

The Deep Sleep power consumption can easily be offset by the solar panel in any decent lighting condition. In case there is no light at all, the onboard battery can still live for months.

A fully charged MS920SE battery is able to continuously power our RF Tag prototype in Permanent Sending mode for a few days in total darkness.

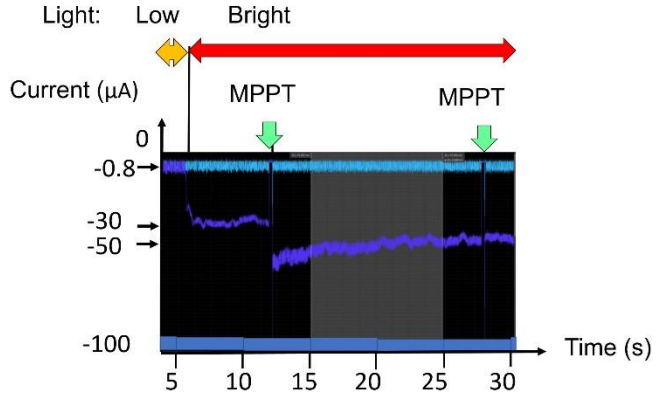

Fig. 8. Current obtained from solar energy harvesting, under varying lighting conditions

Based on this experimental investigation, we can derive the energy model given in Fig. 9 and the expected operating lifetimes listed in Table III.

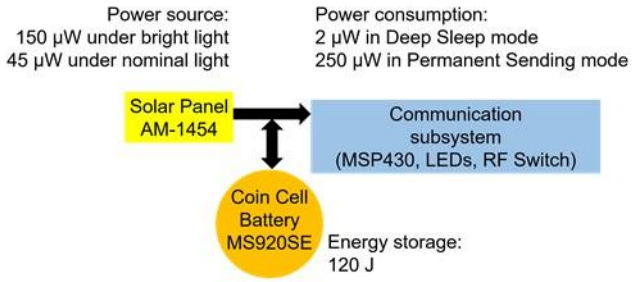

Fig. 9. Simplified energy model of the tag

TABLE III. OPERATING LIFETME ROUGH ESTIMATION, ASSUMING IDEAL 11 MA·H 3.0 V BATTERY, INITIALLY CHARGED

	No Light	Nominal Light	Bright Light
	(0 µW, 24 h/day)	(45 µW, 10 h/day)	(150 µW, 10 h/day)
Deep Sleep Mode (2.3 µW, 24h/day)	1.7 years	infinite	infinite
Permanent Sending (250 µW, 24h/day)	5.6 days	6.0 days	7.4 days
Spaced Sending (54 µW, 24h/day, 10 s period)	22 days	31 days	infinite

To match the use case requirements, the actual RF Tag should operate in a Spaced Sending mode, whereby transmissions are spaced apart. For example, 2.1 s transmissions interspaced with 7.9 s low power mode, i.e., a 10 s transmission period, would allow infinite active lifetime of the RF Tag under bright light and a month under nominal light. More spacing would proportionally increase the lifetime, albeit at the expense of the application liveliness. In our prototype, roughly 2/3^{rds} of the Permanent Sending mode power go into the supply of the RF switch, which we chose for its superior R_{on} and R_{off} values more than for ultra-low operating power. A more power-thrifty RF switch would also significantly increase lifetime of the final tag, albeit potentially at the expense of the communication range. This is the subject of further study.

In any case, the PMIC protects the battery against deep discharge by automatically disabling the output voltage regulator when the battery voltage gets critically low.

This behavior also benefits the application: if a package is left in the dark for an extended period of time, the tag will stop trying to communicate as the battery reaches the low threshold, saving the remaining energy for better times. Quickly after being exposed to light again, the tag will be able to communicate again, instead of needing a long time for bringing the battery from full discharge back up to the operational voltage.

V. FIRST EXPERIMENTS AND DEMONSTRATIONS

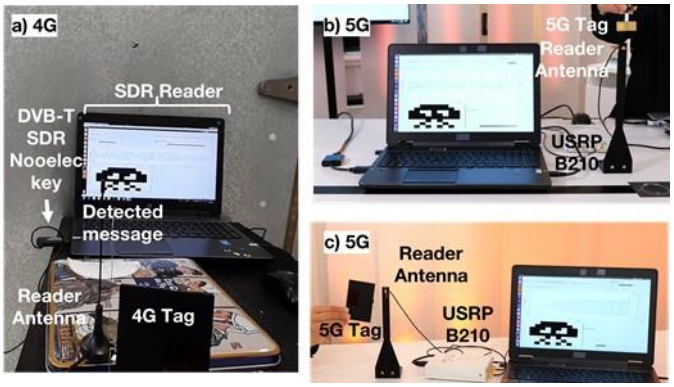

Fig. 10. Ambient backscatter experiment with a) 4G business card size solar tag (**video** [18]), b) 5G tag at 3.65 GHz and Ericsson small cell from Orange 5G commercial network as source GHz (**video** [19]); c) 5G business card size solar tag at 3.65 GHz (**video** [20]).

In this section, we present our first experiments with the compact solar tags presented in Section IV. In these experiments, the tag backscatters ambient signals from TV

towers and 4G or 5G BSs from Orange commercial mobile networks. Our prototype of smartphone (or RF reader) is based on a Software Defined Radio (SDR) GNU platform running on a laptop computer, and initially developed for TV and 4G only, in [4]. Some adaptations presented hereafter, have been introduced to support 5G.

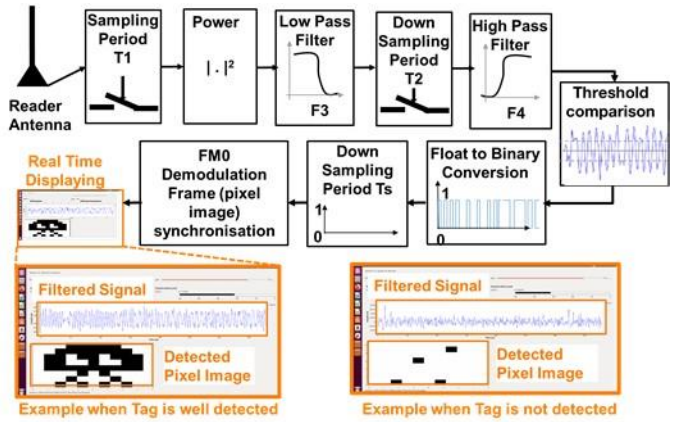

Fig. 11. Reader algorithm with configurable parameters

Two slightly different hardware setups have been designed for low bands (4G around 700 MHz and TV around 500 to 700 MHz) and for high bands (5G at 3.65 GHz). More precisely, as illustrated in Fig. 10-a), our reader for 4G and TV, is connected to an RTL Terrestrial Digital Video Broadcast (DVB-T) SDR Nooelec key connected to a monopole antenna for below 2 GHz bands. As illustrated in Fig. 10-b) and c), our reader for 5G is connected to a Universal Software Radio Peripheral (USRP) B210 board connected to a dipole antenna for 3.65 GHz.

The reader demodulates in real time the tag's message thanks to the simplest signal processing method: the energy-detector or threshold detector used in [2]. The detector can be configured for various ambient sources. More precisely, as illustrated in Fig. 11, this detector samples the received signal with period T1. Then, complex samples are converted into power samples, filtered with a low-pass filter with F3 cut-off frequency, down sampled with period T2, filtered with a high-pass filter with F4 upper cut-off frequency, compared to a threshold (the moving average over a time-window Ta), and converted into binaries ('1' if the sample exceeds the threshold and '0' otherwise). The resulting binary sequence is down sampled with the tag's symbol Ts and demodulated assuming FM0. Finally, the synchronization sequence is detected (by correlation) and the consecutive 88-bit sequence is displayed as an 8-by-11-pixel image. The setting of the reader parameters T1 (F1=1/T1), T2 (F2=1/T2), F3, F4 and Ta are optimized depending on the ambient source, according to Table IV. For 5G, as the traffic is very bursty, Ta/Ts is chosen smaller than for TV and 4G. Note that such detector is non-coherent, without a priori knowledge of the ambient source, and is of low enough complexity to be run in real time on our laptop, as illustrated in filmed experiments [18][19][20].

TABLE IV. PARAMETERS VALUES

Parameter	TV/4G	5G
Ts, Fs	2.7 ms, 370 Hz	10.8 ms (>> T_5G), 93 Hz
2Ts, Fb	5.4 ms, 185 Hz	21.6 ms, 92 Hz
F3 (>Fs), F4 (<Fb)	500 Hz, 50 Hz	100Hz, 1 Hz
T1, F1 (>Fs)	1 µs, 1 MHz	
T2, F2 (>Fs)	0.5 ms, 2 kHz	
Ta (>> Ts)	50 ms	

Fig. 12-a) and b) illustrate indoor experiments with ambient TV and business card size solar tags using a pluggable external dipole antenna (optimized for 540 MHz), at different floors of office buildings. In these experiments, around 4 meters tag-to-reader range was reached with the simplest detector, even though the incoming signal is attenuated by heat-blocking windowpanes. This is because the tag's rate Fb is extremely slow. Also, the experiment was reproduced successfully with the same antenna for various TV channels with carrier frequencies lying between 482 MHz and 700 MHz, confirming that the pluggable dipole antenna tag has a large bandwidth. Finally, Fig. 12-c) and d) illustrates an ambient backscatter communication experiment with ambient TV in challenging conditions: in mobility, underground in a metro train and on board of a high-speed train, respectively.

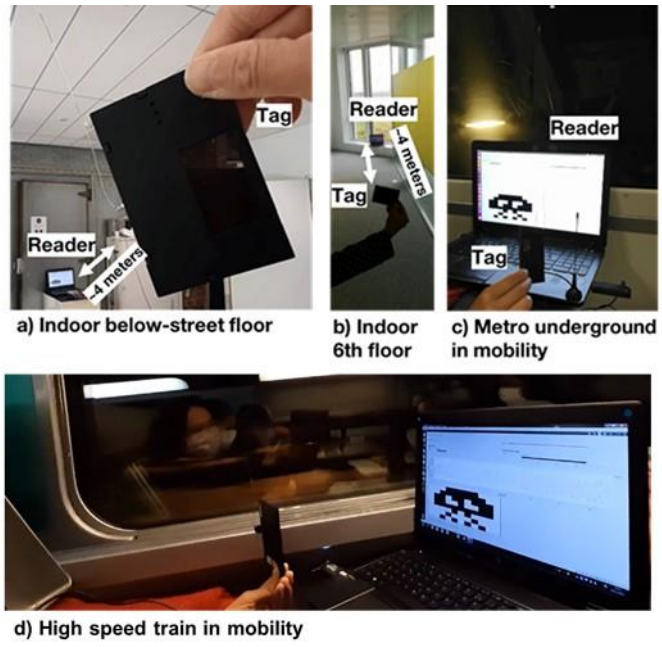

Fig. 12. Ambient TV backscattering experiments in indoor at a) street floor (**video** [21]), and b) 6th floor of an office building (**video** [22]), also in mobility c), underground, in metro train line 13, in a tunnel between Porte de Vanves and Malakoff Plateau de Vanves Stations (**video** [23]), d) on board of a high-speed train between Grenoble and Paris (**video** [24])

VI. First Experimental Feasibility Assessment of Asset-Tracking-Out-of-Thin Air in Various Real Environments

In this section, we perform a first experimental study of the feasibility of the asset-tracking out-of-thin-air use case depicted in Section III. Ideally, to conduct such an experiment, we would need a "reading and localized smartphone" (as illustrated in Fig. 1) with the following capabilities: 1) Reading capability, to detect tags; 2) Self-localization capability, either based on GPS or cellular network position systems. Since this smartphone does not exist, we propose to emulate it by using two co-located devices: 1) our prototype of reader described in Section V, in charge of detecting the tag; 2) a smartphone with a localization app, in charge of self-localization. For the comfort of the reader, we will simply call this emulated "reading and localized smartphone" an "e-smartphone" throughout the rest of the paper.

A. Measurement method

Fig. 13 illustrates our measurement method. For a given measurement, we: 1) set the position of our e-smartphone; 2) pick the coordinates as measured by the smartphone (with a localization app) component of the e-smartphone; 3) determine manually the exact longitude and latitude of our e-smartphone on a map; 4) look for the largest distance *d* between the tag and the reader component of our e-smartphone (at which the tag is detected).

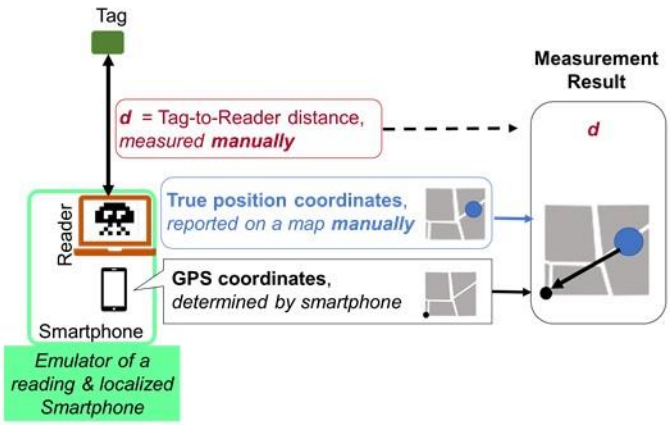

Fig. 13. Sketchup of the measurement method.

Furthermore, as the threshold-detector (described in Section V) performance is too dependent on the Source signal stability, we use TV sources (546 MHz and 642 MHz). Such sources have less bursty data traffic and are close in frequency range to the 4G low band spectrum (at 700 MHz). The obtained results will give us a first indication of the upper-bound performance, that could be obtained with a coherent detector (instead of a threshold detector) for 4G signals.

Finally, during test campaigns we simultaneously tested the two different capabilities of the e-smartphone, in various indoor and outdoor real environments: 1) the ability of the e-smartphone to detect a tag; 2) the ability of the e-smartphone to locate itself and thereby to provide a good approximation of the position of the tag.

To that end, for static configurations, we determine the maximum tag-to-e-smartphone detection ranges, whereas for a tag embedded in a moving vehicle together with an e-smartphone, we determine the maximum car speeds with successful detection. At the same time, we evaluate whether the position of the e-smartphone can be considered as a good approximation of the position of the tag.

B Results in static configurations

We have performed two test campaigns in two following challenging propagation environments: the Langevin Institute area (for outdoor measurements in dense urban environments, at 546 MHz) and the Orange Gardens area (for indoor measurements at various floors of high-rise buildings, surrounded by other close buildings, at 642 MHz).

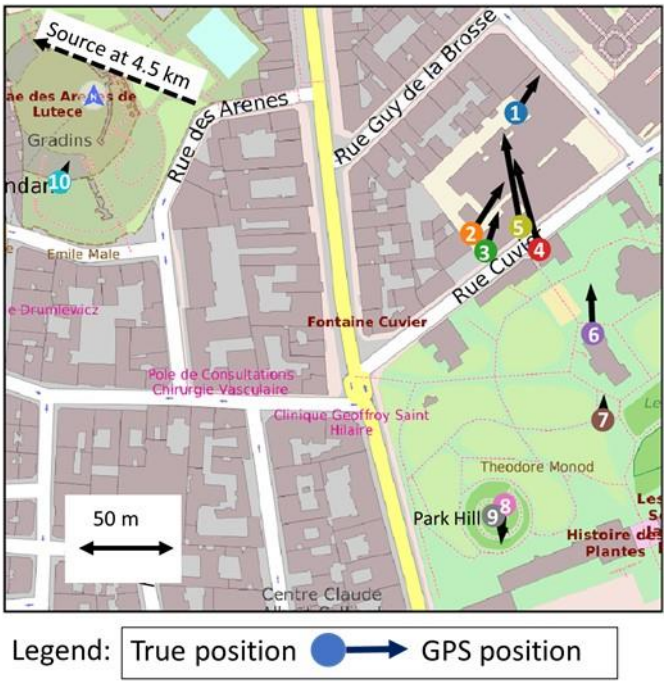

Fig. 14. Map of Langevin Institute neighbourhood, Paris with the positions of the measurements 1 to 10. A circle shows the true position and the extremity of the arrow shows the position provided by the smartphone localisation app.

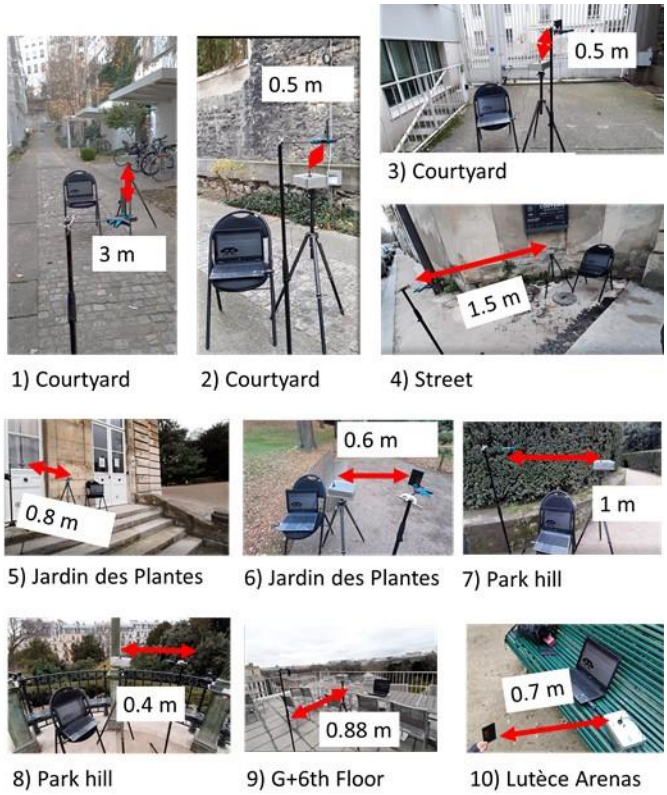

Fig. 15. Pictures corresponding to measurements 1 to 10 performed in Langevin Institute neighbourhood. On each picture is shown the Tag-to-reader distance *d*

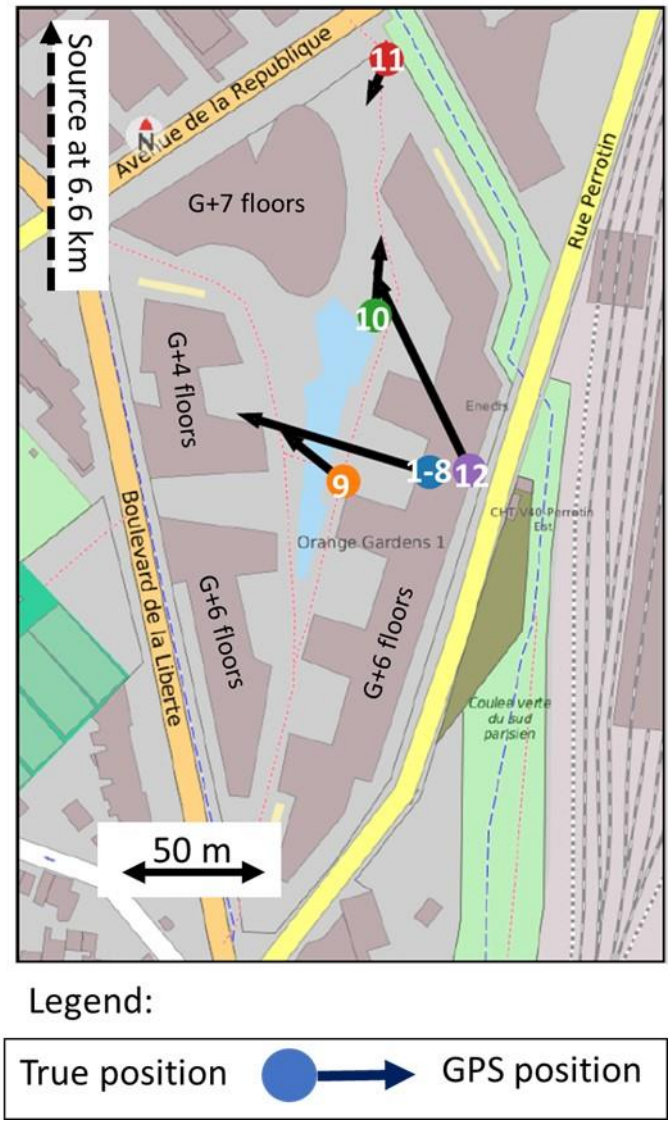

Fig. 16. Map of Orange Gardens area with the positions of the measurements 1 to 12 . A circle shows the true position and the extremity of the arrow shows the position provided by the smartphone localisation app.

As illustrated in Fig. 14, in the Langevin Institute area, smartphone localization errors are in the range of several meters. In comparison, as illustrated in Fig. 15, the maximum tag-to-reader distance is of the order of one meter. As illustrated in Fig. 16, in the Orange Gardens area, due to very close high-rise buildings blocking GPS, the smartphone localization error is also of the order of several meters and can even reach several dozens of meters. In comparison, as illustrated in Fig. 17, the maximum tag-to-reader distance is of the order of one meter. Hence, in these challenging environments, the smartphone localization error is often larger or of the same order of magnitude as the tag-to-reader detection distance. Therefore, associating the position of the smartphone to the tag, to track the tag, as proposed in Section II, is feasible.

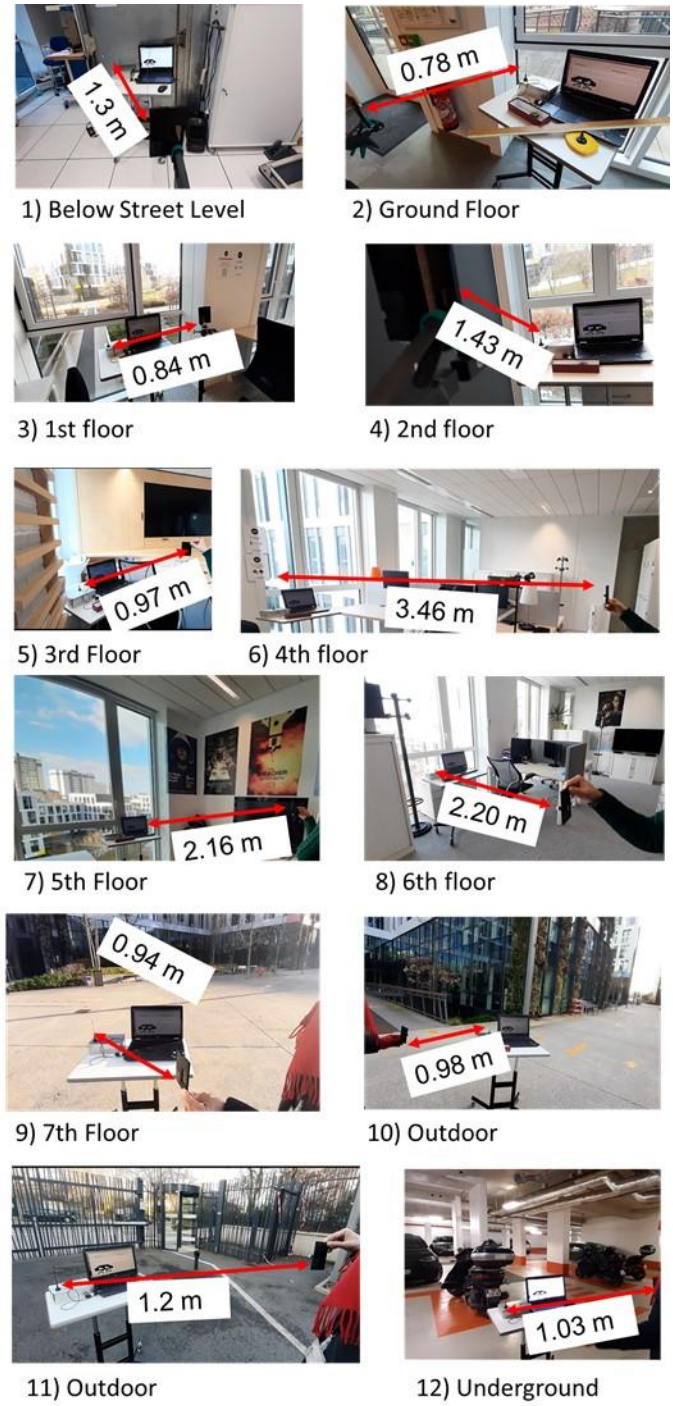

Fig. 17. Pictures corresponding to mesurements 1 to 10 performed in Orange Garden area. On each picture is shown Tag-to-reader distance *d*

Fig. 18 reports the tag-to-reader distances as a function of the received source signal level (in dBm) at the reader side. Note that the effective power radiated by the TV emitters is 47.06 dBW, 46.99 dBW and 33.32 dBW for the results obtained at Langevin Institute, at Orange Gardens, and with the car, respectively. Because of the large distance between the source and the reader and the NLOS configuration, the channel attenuation can reach 150dB. It should be emphasized that even if most of the time the signal level is not sufficient for the receiver to demodulate the TV stream, it is still sufficient for it to demodulate the backscattered FM0 modulation. For a given level, the distance between the tag and the reader varies drastically, as expected, due to the threshold detector algorithm [4]-[5]. Furthermore, as expected, the higher the level, the larger the tag-to-reader distance, on average.

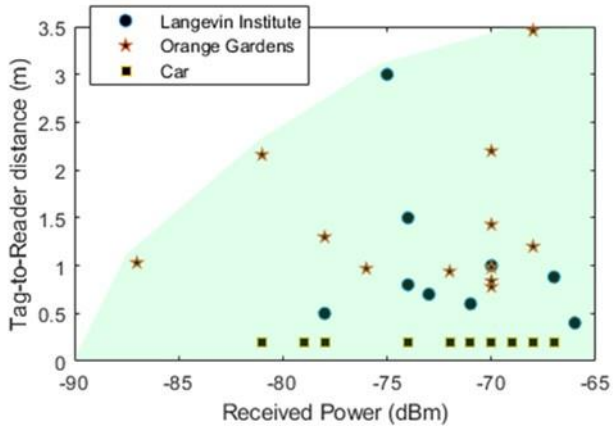

Fig. 18. Tag-to-reader distance *d* versus the signal power level at the reader.

C. Results in mobility

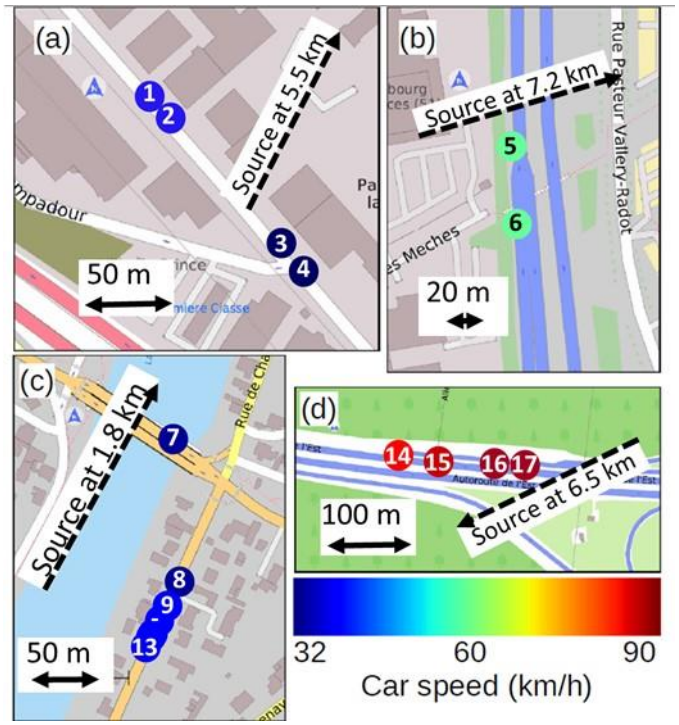

Fig. 19. In-car measurements, on roads of suburban areas (a), (b), (c) and on a highway (d), and corresponding velocities (in color scale).

In Fig. 19 we report measurements performed during drive tests and observe the impact of velocity. In these measurements, the source is again at 642 MHz and the various distances are reported in Fig. 19. The suburban and highway propagation

environment enables good GPS detection. We therefore assume that the smartphone manages to determine the true car position on the road. Furthermore, due to the size of the car, and the size of the set-up, the tag-to reader distance has been constrained to be roughly around 20 to 50 cm (only 20 cm is reported on Fig. 18) for every measurement. As illustrated in Fig. 19, even with the simple threshold detector algorithm, velocities up to 90kmph can be reached. Therefore, the tag could be localized while traveling on board of a fast-moving vehicle, at the condition that a geo-localized smartphone is on-board as well.

Note that this first experimental measurement campaign does not address the challenge of the interaction of smartphones and BSs with different moving tags, which potentially leads to collisions between tags. Though non-orthogonal multiple access (NOMA) in the context of massive IoT [25] has been studied for 5G and beyond, it still remains to be adapted and evaluated in the field for ambient backscatters in mobile networks.

VII. CONCLUSION

In this paper, we have introduced, for the first time, the concept of crowd-detectable zero-energy-devices, also named tags, and the use case of asset-tracking out-of-thin-air. We have presented first prototypes of such devices – business card size solar tags – and tested them with various ambient sources (signals from TV, 4G and 5G ambient commercial networks), and in various conditions, such as indoor and mobility underground. Finally, we have presented first measurement campaigns showing that the position of smartphones in contact with a tag is a good approximation of the tag position and can be used to perform asset-tracking out-of-thin-air. These experiments show that ambient backscattering is a promising technique for mobile networks. Future studies will focus on field trials with improved signal processing algorithms at the reader side, using coherent detection at least, and extension to future 6th generation networks.

VIII. ACKNOWLEDGMENTS

We thank our colleagues M.-A. Mouilleron, P. Legay and G. Tardiveau for their expertise and contributions on use case identification. We thank the Orange teams at the 2021 Orange Labs Research Exhibition and the 2021 Mobile World Congress for their support. We thank our colleagues Frédéric Huet, Guy Salingue, Christophe Simon and Julien Deporcq at Orange, and our colleagues at Ericsson, especially L. Friry, for their help and support on the 5G experiments.

This work has been partially supported by the EU project Hexa-X under EC grant No 101015956.

IX. REFERENCES

[1] A. Gati *et. al*., "Key technologies to accelerate the ict green evolution: An operators point of view", *arXiv:1903.09627*, 2019.

[2] V. Liu, A. Parks., V. Talla, S. Gollakota, D. Wetherall, and J. R. Smith, "Ambient backscatter: Wireless communication out of thin air," in *Proc.SIGCOMM 2013*, 2013.

[3] W. Zhang, Y. Qin, W. Zhao, M. Jia, Q. Liu, R. He, B. Ai, "A green paradigm for Internet of Things: Ambient backscatter communications,"*China Communications*, vol. 16, no. 7, pp. 109-119, 2019.

[4] K. Rachedi, D.-T. Phan-Huy, N. Selmene, A. Ourir, M. Gautier, A. Gati, A. Galindo-Serrano, R. Fara, J. de Rosny "Demo Abstract : Real-Time Ambient Backscatter Demonstration," in *Proc. IEEE INFOCOM 2019*, pp. 987–988, 2019.

[5] K. Rachedi, D.-T. Phan-Huy, A. Ourir and J. de Rosny "Spatial characterization of the ambient backscatter communication performance in line-of-sight," in Proc. 2019 IEEE ISAP and USNC-URSI Radio Science Meeting, Atlanta, Georgia, USA, 7-12 July 2019.

[6] R. Fara, N. Bel-Haj-Maati, D.-T. Phan-Huy, N. Malhouroux, and M. Di Renzo, "First experimental evaluation of ambient backscatter communications with massive MIMO reader," in *Proc. 2020 IEEE PIMRC*, Aug. 2020, pp. 1–6.

[7] R. Fara, D. Phan-Huy and M. Di Renzo, "Ambient backscatters-friendly 5G networks: creating hot spots for tags and good spots for readers," in *Proc.2020 WCNC*, Seoul, Korea (South), 2020, pp. 1-7.

[8] R. Fara, D.-T. Phan-Huy, A. Ourir, M. Di Renzo, and J. de Rosny, "Robust Ambient Backscatter Communications with Polarization Reconfigurable Tags," in *Proc. 2020 IEEE PIMRC*, Aug. 2020, pp. 1–7.

[9] Y. Kokar, D.-T. Phan-Huy, R. Fara, K. Rachedi, A. Ourir, J. de Rosny, M. Di Renzo, J.-C. Prévotet and M. Hélard "First experimental ambient backscatter communication using a compact reconfigurable tag antenna," in *Proc. IEEE Globecom 2019*, Hawaï, USA, Dec. 2019.

[10] R. Fara, D.-T. Phan-Huy, P. Ratajczak, A. Ourir, M. Di Renzo, and J. de Rosny, "Reconfigurable Intelligent Surface -Assisted Ambient Backscatter Communications -- Experimental Assessment," in *Proc. IEEE ICC Workshop on Reconfigurable Intelligent Surfaces for Future Wireless Communications*, 2021, Apr. 2021.

[11] "Crowd-Detectable Zero-Energy-Devices" demonstration at Mobile World Congress, June 28 to July 1st 2021, Barcelona, Spain. Video: https://mastermedia.orange-business.com/publicMedia?t=pmpvq0MMfT

[12] "Energy-Efficient Internet-of-Things" demonstration at 2021 Orange Labs Research Exhibition, march 2021, Chatillon, France. Video: https://hellofuture.orange.com/en/improving-the-energy-efficiency-of-connected-objects/.

[13] 3GPP TS 36.211 V8.9.0 (2009-12) Technical Specification 3rd Generation Partnership Project; Technical Specification Group Radio Access Network; Evolved Universal Terrestrial Radio Access (E-UTRA); Physical Channels and Modulation (Release 8).

[14] 3GPP TS 23.271 V13.1.0 (2017-12) Technical Specification 3rd Generation Partnership Project; Technical Specification Group Services and System Aspects; Functional stage 2 description of Location Services (LCS) (Release 13).

[15] X. Wang, H. Yigitler, R. Duan, E. Y. Menta, and R. Jäntti, "Coherent ¨ multi-antenna receiver for bpsk-modulated ambient backscatter tags," IEEE Internet of Things Journal, 2021.

[16] A. N. Parks, A. Liu, S. Gollakota, and J. R. Smith, "Turbocharging ambient backscatter communication," in Proceedings of the ACM SIGCOMM, Chicago, Illinois, USA, 2014, pp. 619–630.

[17] X. Wang, H. Yiğitler and R. Jäntti, "A Simplified Multi-Antenna Receiver for General Binary-Modulated Ambient Backscatter Signal," 2021 IEEE Global Communications Conference (GLOBECOM), 2021, pp. 1-6,.

[18] "4G Ambient Backscatter Communication experiment with business card size solar tag" https://www.dailymotion.com/video/x82icxv.

[19] "5G Ambient Backscatter experiment"https://www.dailymotion.com/video/x82icrp.

[20] "5G Ambient Backscatter Communication with business card size solar tag". https://www.dailymotion.com/video/x8bh7cj.

[21] "Ambient Backscatter experiment with business card size solar tag, indoor, below street floor", https://www.dailymotion.com/video/x8bh7es.

[22] "Ambient Backscatter experiment with business card size solar tag, indoor, 6th floor" https://www.dailymotion.com/video/x8bh7du.

[23] "Ambient Backscatter communication experiment in Metro with business card size solar tag" https://www.dailymotion.com/video/x82icwo.

[24] “Ambient Backscatter communication experiment in a high speed train with business card size solar tag”. https://www.dailymotion.com/video/x882rbh.

[25] Y. Liu, Z. Qin, M. Elkashlan, Z. Ding, A. Nallanathan and L. Hanzo, "Nonorthogonal Multiple Access for 5G and Beyond," in Proceedings of the IEEE, vol. 105, no. 12, pp. 2347-2381, Dec. 2017.

Dinh-Thuy Phan-Huy [SM] received her degree in engineering from Supelec in 2001 and her Ph.D. degree in electronics and telecommunications from the National Institute of Applied Sciences (INSA) of Rennes, France, in 2015. In 2001, she joined France Telecom R&D (now Orange Innovation), France, where she currently works as a research project manager. Her current research interests include wireless communications and 6G. She is an Orange Expert.

Dominique Barthel graduated from Ecole Polytechnique (1985) and SUPELEC (1987), and currently works with Orange Innovation, Meylan, France. He has been researching architecture and protocols for IoT networks for two decades. He actively contributes to the standardization of IoT protocols at the LoRa Alliance and the IETF, where he co-chairs the ROLL Working Group. Earlier in his career, he architected and designed microprocessors and real-time video processors. He holds 20 patents and is a designated Orange Expert.

Philippe Ratajczak [SM] received his M.Sc. and Ph.D. degrees in electrical engineering from the University of Nice-Sophia Antipolis in 1990 and 1995, respectively. In 1995, he joined CNET (now Orange Innovation Networks), Sophia-Antipolis, France. Since 2014, he has been the co-head of CREMANT, the joint research center on antennas between Orange Innovation, the University of Nice, and CNRS. His research interests include reflectarrays, reconfigurable antennas with beamforming capabilities, and electromagnetic modeling and simulation.

Romain Fara received his Master’s degree in electrical engineering from the National Institute of Applied Sciences of Lyon in 2018 and his Ph.D. degree from CentraleSupelec, Paris-Saclay University, France, in collaboration with Orange Innovation Networks, Chatillon, France, in 2021. His research interests include ambient backscatter communications.

Marco Di Renzo [F] received his Ph.D. degree in electrical engineering from the University of L’Aquila, Italy, in 2007. He is a CNRS research director with the Laboratory of Signals and Systems at Paris-Saclay University, France. He serves as the Editor-in-Chief of IEEE Communications Letters. He is a Fellow of IEEE, IET and AAIA, an ordinary member of the European Academy of Sciences and Arts and the Academia Europaea, a Fulbright Fellow, and a Highly Cited Researcher.

Julien De Rosny received his M.S. and Ph.D. degrees in wave physics from UPMC, Paris, France, in 1996 and 2000, respectively. From 2000 to 2001, he was a postdoctoral fellow with ScriUSA. In 2001, he joined the CNRS at Laboratoire Ondes et Acoustique, France. Since 2014, he has been a CNRS research director with the Institut Langevin, Paris. His research interests include communications in complex media, and acoustic and electromagnetic waves-based imaging.